Dynamical response properties of neocortical neurons to conductance-driven time-varying inputs

Dynamical response properties of neocortical neurons to conductance-driven time-varying inputs

Daniele Linaro[1,2,*], István Biró [2,*], Michele Giugliano[2-4]

[1] *IRIBHM, Université Libre de Bruxelles, Brussels, Belgium*
[2] *Theoretical Neurobiology & Neuroengineering, University of Antwerp, Antwerp, Belgium*
[3] *Department of Computer Science, University of Sheffield, S1 4DP Sheffield, UK*
[4] *Lab of Neural Microcircuitry, Brain Mind Institute, EPFL, CH-1015 Lausanne, Switzerland*

Correspondence should be addressed to Dr. Michele Giugliano, Theoretical Neurobiology and Neuroengineering, University of Antwerp, Campus CDE, Universiteitsplein 1, 2610 Wilrijk, Belgium. E-mail: michele.giugliano@uantwerpen.be

Author contributions: Conceived and designed the experiments: D.L. and M.G. Performed the experiments: D.L. and I.B. Analysed the data: D.L. and I.B. Contributed reagents/materials/analysis tools: M.G. Wrote the paper: D.L., I.B., and M.G. Equally contributing authors: D.L. and I.B.

Data accessibility statement: Authors confirm that the data underlying their findings are fully available. Relevant data sets and analysis scripts have been stored at FigShare.com (doi10.6084/m9.figshare.4822852), including an index of the deposited data.

Abstract

Ensembles of cortical neurons can track fast-varying inputs and relay them in their spike trains, far beyond the cutoff imposed by membrane passive electrical properties and mean firing rates. Initially explored *in silico* and later demonstrated experimentally, investigating how neurons respond to sinusoidally-modulated stimuli provides a deeper insight into spike-initiation mechanisms and information processing than conventional F-I curve methodologies. Besides net membrane currents, physiological synaptic inputs can also induce a stimulus-dependent modulation of the total membrane conductance, which is not reproduced by standard current-clamp protocols.

Here we investigated whether rat cortical neurons can track fast temporal modulations over a noisy conductance background. We also determined input-output transfer properties over a range of conditions, including: distinct presynaptic activation rates, postsynaptic firing rates and variability, and type of temporal modulations. We found a very broad signal transfer *bandwidth* across all conditions, similar large cutoff frequencies and power-law attenuations of fast-varying inputs. At slow and intermediate input modulations, the response gain decreased for increasing output mean firing rates. The gain also decreased significantly for increasing intensities of background synaptic activity, thus generalising earlier studies on F-I curves. We also found a direct correlation between the action potentials' onset rapidness and the neuronal bandwidth. Our novel results extend previous investigations of dynamical response properties to non-stationary and conductance-driven conditions, and provide computational neuroscientists with a novel set of observations that models must capture when aiming to replicate cortical cellular excitability.

Introduction

The rapidity by which a single cortical neuron relays time-varying information from its input to its output spike train has an upper biophysical limit. This limit is roughly determined by its passive membrane properties and by its mean inter-spike interval. However, it is well established that, as ensembles, neurons can overcome such limitations and transfer rapidly oscillating input components downstream, without any significant attenuations. This phenomenon is also reflected in the extremely fast population reaction times to input transients, when the innate low-pass filtering properties of isolated single cells are boosted by a form of "*team-work*". These properties have been investigated extensively in theoretical (*e.g.* see Brunel *et al.,* 2001; Brunel *et al.,* 2003; Brunel and Wang, 2003; Fourcaud-Trocmé *et al.,* 2003; Fourcaud-Trocmé and Brunel, 2005; Naundorf *et al.,* 2005) and experimental studies (*e.g.* Köndgen *et al.,* 2008; Tchumatchenko *et al.,* 2011; Wei and Wolf, 2011; Ilin *et al.,* 2013; Testa-Silva *et al.,* 2014). On a first approximation, the larger a population the greater the advantage of a broad heterogeneity of electrical activity across its cells during asynchronous spiking regimes. For instance, during sparsely synchronised network rhythms (reviewed in Wang, 2010), an individual neuron experiences a periodically-varying net synaptic drive, while it still may fail to fire an action potential (AP) during every single oscillation period. Other cells however, which are closer at the same moment to their own firing threshold than that neuron, may fire instead. Therefore, presynaptic rhythms and rapidly varying signal components can be conveyed downstream through time-varying collective firing rates. This mechanism could be essential for the emergence (and self-sustenance) of brain rhythms (Wang, 2010; Buzsaki and Draguhn, 2004), particularly when cells fire sparsely and at much lower mean rates than the dominant Fourier frequency of the associated local field potentials (*e.g.* Brunel and Wang, 2003; Geisler *et al.,* 2005; Wang, 2010). Thus, the accurate measurement of these collective transfer properties in single cells is crucial for dissecting the biophysical information processing in cortical networks.

Previous experimental studies have been particularly useful for challenging existing mathematical models of action potential (AP) initiation: they all reported very large cutoff frequencies of ~200–400 cycles/s in rodents (Köndgen *et al.,* 2008; Boucsein *et al.,* 2009; Ilin *et al.,* 2013; Tchumatchenko *et al.,* 2011) and much larger in human cortical neurons (Testa-Silva *et al.,* 2014). Other studies have linked this broad band transfer to the onset rapidity of action potentials in mathematical models (Fourcaud-Trocmé *et al.,* 2003; Ilin *et al.,* 2013) and experiments (Naundorf *et al.,* 2006; Testa-Silva *et al.,* 2014). However, only current-clamp stimuli have thus far been employed for recreating *in vivo*-like firing regimes *in vitro* (Giugliano *et al.,* 2008; La Camera *et al.,* 2008) in the context of dynamical response properties. While postsynaptic currents are the ultimate contributors to information processing, physiological inputs are mediated by ionic conductances that also produce a marked simultaneous effect on the cell input resistance. Indeed, quantitative differences are expected to occur in neuronal responses when comparing *in vivo*-like current- and conductance-driven fluctuating regimes (Tiesinga *et al.,* 2000; Destexhe *et al.,* 2001; Chance *et al.,* 2002; Destexhe *et al.,* 2003), but see (La Camera *et al.,* 2004). A recent study (Litwin-Kumar *et al.,* 2011) suggested (despite its paucity of experimental data), that care should be taken when comparing dynamical responses based on current- *versus* conductance-driven inputs.

To extend the previous experimental efforts to more physiologically plausible settings, we investigated the input-output dynamical transfer properties of rat cortical L5 pyramidal neurons *in vitro* by dynamic-clamp. Unlike previous attempts where input mean and variance were modulated independently (Boucsein *et al.,* 2009; Tchumatchenko *et al.,* 2011), here we used a biophysically-realistic setup in which the main free input parameter was the firing rate of the emulated presynaptic population(s), thus controlling simultaneously mean and variance. Neuronal responses were investigated under a recreated barrage of irregular synaptic background events as observed *in vivo* (Destexhe *et al.,* 2003), with the information-carrying signal realized either as a superimposed current waveform (as in Chance *et al.,* 2002) or as a modulation of the rate of either or both the synthetic presynaptic populations.

Materials and Methods

Brain tissue slice preparation. Experiments were performed as described previously (Köndgen *et al.,* 2008) and in accordance with international and institutional guidelines on animal welfare. All procedures were approved by the Ethical Committee of the University of Antwerpen (permission no. 2011_87) and licensed by the Belgian Animal, Plant and Food Directorate-General of the Federal Department of Public Health, Safety of the Food Chain and the Environment (license no. LA1100469). Briefly, Wistar rats of either sex (2–3 weeks old) were anesthetized using Isoflurane (IsoFlo, Abbott, USA) and decapitated. Brains were rapidly extracted and immersed in ice-cold Artificial CerebroSpinal Fluid (ACSF), containing (in mM): 125 NaCl, 25 $NaHCO_3$, 2.5 KCl, 1.25 NaH_2PO_4, 2 $CaCl_2$, 1 $MgCl_2$, 25 glucose, saturated with 95% O_2 and 5% CO_2, and having pH 7.3 and osmolarity of ~315 mOsm. Parasagittal sections ($300\ \mu m$ thick) of the primary somatosensory cortex were cut using a vibratome (VT1000 S, Leica Microsystems GmbH, Germany) and were subsequently incubated in ACSF at 36℃ for 45 minutes. Slices were then stored at room temperature, until transfer to the recording chamber.

Layer 5 (L5) cortical pyramidal cells, with a thick apical dendrite (McCormick *et al.,* 1985), were visualized using an upright microscope (SliceScope, Scientifica, UK, or DMLFS, Leica Microsystems) using infrared differential interference contrast microscopy (DIC), in a submerged slice recording chamber, under 40× or 60× magnification. Experiments were performed at a temperature of 32 ± 1℃, under continuous perfusion with ACSF at a rate of $1\ mL/min$. All chemicals were obtained from Sigma-Aldrich (Diegem, Belgium).

Electrophysiological recordings. Whole-cell patch clamp recordings were obtained from the soma of L5 pyramidal cells, using filamented borosilicate glass pipettes (World Precision Instruments, USA) prepared with a micropipette horizontal puller (P-97, Sutter Instruments, Novato, USA). Pipette electrode resistance was in the range $4 - 9\ M\Omega$, when filled with an intracellular solution containing (in mM): 115 K-gluconate, 20 KCl, 10 4-(2-hydroxyethyl)-1-piperazineethanesulfonic acid (HEPES), 4 adenosine triphosphate-Mg, 0.3 Na_2-guanosine triphosphate, 10 Na_2-phosphocreatine, pH adjusted to 7.3 with KOH and having an osmolarity of ~290 mOsm. Recordings and current injections were performed with a single electrode, using either an Axon Multiclamp 700B Microelectrode Amplifier (Molecular Devices, USA) or an EPC 10 patch clamp amplifier (HEKA Electronics, Lambrecht/Pfalz, Germany) in current-clamp mode, controlled by a personal computer running a real-time operating system: either xPC and Simulink (The MathWorks, Natick, USA) (Biro & Giugliano, 2015) or real-time Linux (Linaro *et al.*, 2014).

Recorded voltage waveforms (or external current commands) were sampled (or synthesized) at frequencies of 15 or 20 kHz and A/D (D/A) conversion resolution of 16 bit, with an electronic board (NI PCI-6221, National Instruments, USA). Neither bridge balance nor capacitance neutralisation was used *online*. Instead, signal transfer properties of each glass microelectrode were repeatedly estimated throughout the recording session by a linear non-parametric identification method (Brette *et al.,* 2008). Quantified in terms of the impulse response, the transfer properties of glass electrodes were employed to compensate for artifacts in the recorded membrane potential offline or online (*i.e.* in conductance-clamp experiments). Data from N=186 L5 pyramidal neurons were included in this study: cells had input resistance of 52.4 ± 25 MOhm, capacitance of 470 ± 183 pF, and membrane time constant of 21 ± 5.6 ms, determined as described previously (Köndgen *et al.,* 2008). All numerical data are presented as the mean ± standard deviation, unless otherwise noted.

Current-clamp and conductance-clamp stimulation. *In vivo*-like activity was recreated *in vitro* by emulating background synaptic activity as fluctuating somatic input conductances (Destexhe *et al.,* 2001). The current $I(t)$ injected into a neuron was computer-generated in real time by dynamic-clamp (Biro and Giugliano, 2015; Linaro *et al.,* 2014; Bal and Destexhe, 2009; Destexhe *et al.,* 2003; Economo *et al.,* 2010; Robinson and Kawai, 1993) as

$$I(t) = G_E(t)\big(E_E - V(t)\big) + G_I(t)\big(E_I - V(t)\big), \quad (1)$$

where $G_E(t)$ ($G_I(t)$) represents the amplitude of a randomly fluctuating excitatory (inhibitory) synthetic synaptic conductance, whose apparent reversal potential is chosen as $E_E = 0\,mV$ ($E_I = -80\,mV$), and where $V(t)$ is the membrane potential instantaneously recorded from the cell.

The excitatory (inhibitory) conductance waveform $G_E(t)$ ($G_I(t)$) evolved in time randomly (and independently), as a result of the asynchronous activation of a large number of simulated presynaptic afferents, each with peak synaptic conductance g_E (g_I) and exponential decay τ_E (τ_I) and collectively activated as a stationary Poisson point process $\{t_k\}$ with rate parameter R_E (R_I). Dropping the suffix E or I, for the sake of simplicity of notation, we define

$$\tau \frac{dG(t)}{dt} = -G(t) + g\,\tau \sum \delta(t - t_k). \quad (2)$$

Such a waveform was numerically generated as a realisation of an independent Ornstein-Uhlenbeck stochastic process (Uhlenbeck and Ornstein, 1930), using the diffusion approximation (Bal and Destexhe, 2009):

$$\tau \frac{dG(t)}{dt} \approx -G(t) + g\,\tau\,R + g\,\tau\,\sqrt{R}\,\xi(t), \quad (3)$$

where $\xi(t)$ is a realization of a delta-correlated independent Gaussian white noise, with zero mean and unitary variance. We followed the convention introduced by (Chance *et al.,* 2002) and set the value of g_E (g_I) as 2% (6%) of the total neuronal membrane conductance measured for each cell. The values for the synaptic decay time constants were chosen as $\tau_E = 5\,ms$ and $\tau_I = 10\,ms$, mimicking fast ionotropic glutamatergic and GABAergic synaptic transmission.

To explore the impact of weak or strong background synaptic activity, we chose two distinct values for the excitatory presynaptic activation rate R_E: 7 or 14 kHz. The value of the inhibitory presynaptic activation rate R_I was instead chosen according to

$$R_I = R_E\,\frac{g_E\,\tau_E\,(V_b - E_E)}{g_I\,\tau_I\,(E_I - V_b)}, \quad (4)$$

where V_b is the value at which the mean excitatory and inhibitory components of the injected current cancel each other, *i.e.,* the cell is in the "balanced" state (Chance *et al.,* 2002; Abbott and Chance, 2005).The value of V_b was chosen close to the firing threshold of the neuron, leading to a very low output mean firing rate, in the range $1 - 2\,Hz$.

We then investigated the dynamical input-output response properties of neurons, extending our previous work (Köndgen *et al.,* 2008). Firstly, we investigated the immediate generalization of (Chance *et al.,* 2002) and (Köndgen *et al.,* 2008), where a time-varying input current waveform is injected while the neuron experiences stationary background conductance fluctuations (Eq. 5):

$$I(t) = I_0 + I_1 \sin(2\pi f t) + G_E(t)\big(E_E - V(t)\big) + G_I(t)\big(E_I - V(t)\big), \quad (5)$$

where I_1 and f are the amplitude and the oscillation frequency of a sinusoidal current term, and I_0 is an offset current, whose value was chosen to drive the cells at low ($3 - 9\,Hz$) or high ($15 - 25\,Hz$) output mean firing rates.

Secondly, we employed a more biophysically realistic scenario, using Eq. 1 instead of Eq. 5 and imposed non-stationary background conductance fluctuations by setting

$$R(t) = R_0 + R_1 \sin(2\pi f t). \quad (6)$$

In fact, when R_E and/or R_I in Eq. 3 become time-varying (*i.e.* with identical oscillation frequency *f* but not necessarily identical offsets and amplitudes), the two independent Ornstein–Uhlenbeck processes corresponding to $G_E(t)$ and $G_I(t)$ become non-stationary. Note that in this instance Eq. 4 was still used but only applied to $R_{I\,0}$ and to $R_{E\,0}$.

Finally, we aimed to isolate synaptic and neuronal intrinsic filtering properties and thus considered a simpler case, by using Eq. 1 while replacing Eq. 3 by

$$\tau \frac{dn(t)}{dt} \approx -n(t) + \sqrt{2\tau}\,\xi(t) \qquad G(t) = g\,\tau\,R(t) + g\,\sqrt{\tau\,R(t)}\,n(t) \tag{7}$$

for generating the excitatory (inhibitory) conductance waveform $G_E(t)$ ($G_I(t)$) (*i.e.* using two independent realisations of *n(t)*). When the stationary case is considered (*i.e.* $R_1 = 0$ or $f \to 0$), Eqs. 3 and 7 lead to identical statistical and spectral properties for the corresponding stochastic processes. Otherwise, the power spectra of the processes generated by Eqs. 3 or 7 differ by an amplitude $\sim 1/\sqrt{1+(\pi f \tau)^2}$ that represents the inherent low-pass filtering operated by the model of synaptic transmission of Eq. 2. In the deterministic case (*i.e.* $n(t) = \xi(t) = 0$), the conductance waveforms generated by Eqs. 3 or 7 differ by the (complex) factor of $1/\,[1 + \tau\, j\, 2\,\pi\, f]$.

Following a well-characterized framework in dynamical systems theory, the amplitude of input modulations (I_1 or R_1) was kept small (*i.e.* 5–20% of the respective offset, being I_0 or R_0) to maintain the neuronal response in a linear regime, with negligible harmonic components (Fourcaud-Trocmé *et al.,* 2003).

Data analysis and statistics: instantaneous firing rate. Recorded traces were analysed using custom MATLAB scripts (The MathWorks, Natick MA, USA) as described by Köndgen et al. (2008). Briefly, the times of occurrence $\{t_q\}$ of the spikes fired by the neuron were detected by finding the peaks of the intracellular voltage traces exceeding a threshold of $-20\,mV$. The instantaneous output firing rate $r(t)$ was estimated by first referring the spike times over one period of the input oscillation (*i.e.* $\{t_q \bmod f^{-1}\}$) (Fig. 1D) and then computing the peri-stimulus spike time histogram (Fig. 1E) with bin size equals to one tenth of the input period. A first-order approximation of the neuronal dynamical response was best fit on the histogram according to

$$r(t) \approx r_0 + r_1(f)\sin\big(2\pi f t + \varphi(f)\big), \tag{8}$$

identifying mean r_0, modulation amplitude $r_1(f)$, and phase $\varphi(f)$ of the output firing rate. Throughout this paper, the modulation amplitude is reported and graphically represented after normalizing it by the mean (*i.e.* $r_1(f)/r_0$) and referred to as response *magnitude* or *gain*.

In our experiments, we explored the range $1 - 1000\,cycles/s$ for the input oscillation frequency *f*. Given our choice of parameters, cells' output firing rates and inter-spike interval distributions for stationary inputs, we found that spike trains lasting $40 - 90\,s$ were necessary for reliably estimating $r_1(f)$ and $\varphi(f)$, for each value of *f*.

We then normalised $r_1(f)$ by the value of r_0 and computed its level of significance by repeating the same analysis on surrogate data. Briefly, for each acquired spike train a set of 100 surrogate trains was obtained, by randomly shuffling the original inter-spike intervals (Ilin *et al.,* 2013): mean r_0, modulation amplitude $r_1(f)$, and phase $\varphi(f)$ were best fit on each of the 100 histograms obtained, and individually averaged for the same frequency *f* to obtain a mean value and a level of minimal significance, defined as the sum of one standard deviation and the mean values.

Finally, despite periodic with period of 2π by definition, the phase $\varphi(f)$ was unwrapped to produce smoother plots and emphasize the presence of a linear dependency on f (Köndgen *et al.,* 2008; Fourcaud-Trocmé *et al.,* 2003).

Data analysis and statistics: phenomenological model. Consistent with the theory of linear dynamical systems, we concisely expressed the modulation amplitude and phase of the output firing rate experimentally identified by a phenomenological model (Köndgen *et al.,* 2008). Briefly, $r_1(f)/r_0$

and $\varphi(f)$ were taken as the magnitude and phase of the impulse response of a linear filter in cascade with a delay line, which is completely described by a high order input–output ordinary differential relationship. In Fourier's domain, this takes the form of a complex-valued rational polynomial function, called transfer function,

$$H(f) = A \cdot \frac{\prod_{i=1}^{M}(j\,2\pi f + z_i)}{\prod_{i=1}^{N}(j\,2\pi f + p_i)} \cdot \frac{\prod_{i=1}^{N} p_i}{\prod_{i=1}^{M} z_i} \cdot e^{-j2\pi f \Delta t}, \quad (9)$$

where $j = \sqrt{-1}$ is the imaginary unit, A is known as the low-frequency *gain*, Δt is a fixed time delay, and $\{p_i\}$ and $\{z_i\}$ are called *poles* and *zeros* of the transfer function, respectively. These poles and zeros are the roots of the complex polynomials at the numerator and denominator of $H(f)$, and allow the objective definition of the cutoff frequencies that are associated with high-pass, band-pass, or low-pass behaviours of interest in the neuronal response. In the following experiments, we shall use the term *cutoff (low-pass) frequency* to indicate the largest absolute frequency pole in Eq. 9. We fit Eq. 9 to both single-cell data and population averages, identifying the free parameters A, Δt, $\{p_i\}$, and $\{z_i\}$, but searching for the minimal number of poles and zero with the constraint M < N, thus ensuring causality of the transfer function. For the single-cell data set, the mean-square error between experiment and prediction by Eq. 9 was minimised while weighing it by the inverse of the confidence interval, returned for each frequency *f* by the MATLAB routine employed to fit the peri-stimulus spike time histogram. In the case of population data, the mean-square error was instead minimised while weighing it by the inverse of the standard deviation of data points across cells for the same frequency *f*.

We found that our data could be best fit using a single *zero* (*i.e.* $M = 1$), usually located at very low frequencies, and two or three *poles* (*i.e.* $N = 2,3$). The numerical value of the largest *pole* provides a measure for the (low-pass) cutoff frequency and it has been graphically localised on each related subplot as a vertical line. In addition, in the limit of very high input oscillation frequency *f*, this also automatically accounts for the power-law decay f^{α} observed experimentally in the amplitude modulation, whose exponent $\alpha = M - N = -1, -2$, was previously linked to the non-linearity of spike initiation, in theoretical and experimental studies (Köndgen *et al.,* 2008; Fourcaud-Trocmé *et al.,* 2003).

Finally, the best fit value of the delay Δt has been previously linked to the AP width and to the distal location of action potential generation, *i.e.* in the axon initial segment (Köndgen *et al.,* 2008). Tables 1-2 provide the best-fit parameters corresponding to the population summaries of Figs. 6-7.

Data analyses: AP rapidness. We conventionally defined the threshold of individual APs by the value of membrane voltage corresponding to the maximum of the third time derivative of the membrane potential as described by Henze and Buzsaki (2001). The AP rapidness was then computed as the slope of the line tangent to the AP trajectory plotted in the plane V_m *versus* dV_m/dt, at the voltage coordinate corresponding to the AP threshold. This amounted to values of dV_m/dt in the range $(10 - 30\ ms^{-1})$, which are in line with previous reports (Naundorf et al. 2006). For each cell, we extracted a single value of AP onset rapidness by the grand average of the onset rapidness out of only the first two APs emitted in each stimulation trial, as the cell received fluctuating conductance inputs.

Step-changes in the presynaptic firing rate. To measure the response to an abrupt increase in the activation rate of the presynaptic populations, we step-changed the instantaneous rate of the presynaptic excitatory population while keeping the rate of the presynaptic inhibitory population stationary. In other words, in Eq. 7 we set $R(t) = R_{E\,0}$ for $t < 0$, and $R(t) = \gamma\, R_{E\,0}$, with $\gamma > 1$ for $t > 0$, with $t = 0$ being the step onset. Both $R_{E\,1}$ and $R_{I\,1}$ were kept constant and equal to 0. For this set of experiments, we only considered the regime of low output mean firing rate, high coefficient of variation of the inter-spike interval distribution (CV), and strong synaptic background, and we instantaneously increased the steady-state value of the excitatory firing rate by 5 or 10% (*i.e.* $\gamma \in \{1.05;\ 1.1\}$). The stimulus was applied for at least $500\ ms$ before and after the step change in

presynaptic firing rate, to ensure the steady-state of the cell's firing rate and to minimize adaptation effects. In total, n=16 neurons were used and each cell was stimulated with at least N independent repeated trials. Step-onset detection was performed exactly as described in (Tchumatchenko *et al.,* 2011).

Results

Neuronal output transfer of time-varying inputs. We describe the patch-clamp electrophysiological data collected from 186 layer 5 pyramidal neurons in acute tissue slices of somatosensory cortex of juvenile rats. *In vivo*-like irregular activity was recreated *in vitro* by the dynamic-clamp technique (Fig. 1), following a standard method. This proceeds by emulating the irregular activation of presynaptic inputs as randomly fluctuating synthetic excitatory and inhibitory input conductance waveforms, injected in real-time into the neurons. Instead of examining the neuronal response to fluctuating inputs with stationary statistics (*e.g.* Chance *et al.,* 2002; La Camera *et al.,* 2008), we rapidly varied the input (Fig. 1A-C) to probe the dynamics of input–output transfer properties. We employed four distinct ways for delivering sinusoidally oscillating small-amplitude input modulations to the neurons, and consistently use the labels $\{\Delta I\}$, $\{\Delta R_E\}$, $\{\Delta R_I\}$, and $\{\Delta R_E, \Delta R_I\}$ for further clarity. These types of input modulations (i-iv) consist in alternatively:

i) $\{\Delta I\}$ – injecting an additional sinusoidal current-clamp waveform (Fig. 1A; see Eqs. 3,5) to the fluctuating conductance background, thus extending Chance *et al.*, 2002;
ii) $\{\Delta R_E\}$ – weakly modulating the activation rate of either excitatory (Fig. 1B; Eqs. 1,7) or
iii) $\{\Delta R_I\}$– inhibitory presynaptic synthetic inputs, or
iv) $\{\Delta R_E, \Delta R_I\}$ – both simultaneously (Eqs. 1,7), thus generalising Köndgen *et al.,* 2008.

Using the (ii) – $\{\Delta R_E\}$ protocol (Fig. 1B-C), a sample net excitatory conductance $G_E(t)$ can be computer-synthesised as a realization of a random stochastic process as displayed as the top trace of Fig. 2A: both its mean and variance change rapidly in time, following the small-amplitude sinusoidal modulation of the excitatory activation rate $R_E(t)$. To this conductance-driven input, neurons responded by firing sparsely in individual trials (Fig. 2A, lower trace), but as the spike times are analysed over successive input cycles (Fig. 2B) the instantaneous output firing probability estimated by the peri-stimulus time histogram (Fig. 2C) revealed a prominent output temporal modulation. This occurs at the same frequency *f* of the input sinusoid up to *300 cycle/s* in the representative neuron of Fig. 2, above which they become strongly attenuated. Also for very slow modulations, the exemplary neuron shown responded with a strong attenuation. Note that the neuron does not stop firing, but maintains the same output mean firing rate. These output oscillations are quantified in terms of mean, magnitude, and phase (Fig. 2C) and, as demonstrated in four panels of Fig. 2C, vary depending on the value of *f*. Their systematic characterisation (*i.e.* over *f = 1 – 1000 cycle/s*) is akin to an electronic "filter", *i.e.* possessing *bandwidth*, *high-* or *low-pass* properties, and a *cutoff* frequency.

When considering the (ii) – (iv) protocols, the setup of Fig. 2B is biophysically highly realistic. However, they unavoidably induce an additional upfront attenuation and phase shift "in cascade" to the neuronal transfer (see Eq. 3), caused by our design of non-instantaneous kinetics of individual synaptic excitatory and inhibitory conductances ($\tau_E = 5ms$, $\tau_I = 10ms$). This effect is present *e.g.* in the red fluctuating trace of $G_E(t)$ of Fig. 1B's cartoon (red trace), but it cannot be visually appreciated as *f* is small in that example. The higher *f*, the stronger the attenuation in the conductance waveforms ($G_E(t)$ and/or $G_I(t)$) injected in the neuron. In other words, the power of the input modulations that are faster than the synthetic synaptic time constants (*i.e.* $f \gg 1/(2\,\pi\,\tau)$) is attenuated by a factor $\sim 1/f$ before injection into the cell. This in fact corresponds to the effect of a low-pass filter, with very low cutoff frequency ($(2\pi\tau_E)^{-1} = 31.8\,cycle/s$, $(2\pi\tau_I)^{-1} = 15.9\,cycle/s$), and it is represented by the black dotted lines in Fig. 3 that represent magnitude and phase of the complex function $1/[1 + \tau\, j\, 2\,\pi\, f]$, describing theoretically the synapses.

In this study, we aimed to isolate only the cell's intrinsic contribution to the dynamical transfer properties, by measuring magnitude and phase of the neuronal instantaneous output firing rate at the highest signal-to-noise ratio possible across all input sinusoidal frequencies *f*. We then devised a modification of the setup of Fig. 1B and turned it into 1C, *i.e.* we used Eq. 7 instead of Eq. 3 (see the Methods), to carefully compensate for the synaptic filtering, without altering the spectral properties of the recreated synaptic fluctuations. Figure 3 illustrates this important methodological step, plotting the measured dynamical transfer properties – as normalised magnitude and phase – and comparing the experimental results obtained with or without the unwanted synaptic filter. This was performed considering the (ii) and (iii) protocols, modulating alternatively the excitatory ($\{\Delta R_E\}$; warm colours; left panels) or the inhibitory activation rate ($\{\Delta R_I\}$; cold colours; right panels), and setting $R_{E0} = 7\ kHz$ and R_{I0} as in Eq. 4. As expected, if synaptic filtering is left uncompensated (light-coloured markers and dashed lines), its attenuation precludes investigating the effects of modulations faster than 30 or 15 cycles/s.

Figures 4 and 5 demonstrate our entire data set, plotting population summaries of cells' intrinsic dynamical responses, employing different input modulation protocols *i.e.* (i) - (iv) (row-wise) and exploring various activity regimes (column-wise), which will be introduced and examined in the next sections (see also the Supplemental Material, Fig. S1). Each subplot of Figs. 3, 4,and 5 displays for each value of *f* the normalised magnitude and phase of the neuronal response, averaging over many cells, with markers and error bars indicating mean ± s.e.m., respectively. Black dashed lines in Fig. 4 represents the minimal significance levels of the output modulation, and red dashed lines are best-fits of the simplest power-law (*i.e.* Bf^{α}), with the value of the exponent α indicated above each panel, along with the number of cells considered in each condition. In most cases, it was possible to record more than one transfer function per cell, across different conditions. Horizontal dashed grey lines in Fig. 5 emphasize the location of phase 0 or $-\pi$ and the individual insets zoom in over input modulations. The value of the parameter Δt (see Methods) derived from the slope of the curve is specified above each panel, along with the number of cells considered in each condition.

From the results shown in Figs. 3-5, we outline the key features of the intrinsic neuronal dynamical response: (*a*) a broad bandwidth (up to 200–400 cycles/s), (*b*) a power-law attenuation f^{α} for very fast input modulations, with negative exponents (-1.23 $\pm$ -0.15, range [-1.5; -0.9] (see also Fig. 4), (*c*) a phase-advance for slow input modulations *f* (referred to 0 or to $-\pi$, for excitatory or inhibitory modulations, respectively), and (*d*) a non-saturating linear phase decrease for large *f* (Fig. 3C-D; Fig. 5). In Figs. 3-4, continuous coloured lines demonstrate best-fit plots of the response of a phenomenological model (see the Methods), which captures simultaneously the magnitude and phase of the neuronal dynamical responses with only 6 free parameters (see Tables 1-2), and allows for unbiased estimates of magnitude, cutoff frequencies (see Methods), and propagation delays.

Our data demonstrate that the output modulation remains above the minimal significance level across f = 1-1000 cycles/s, indicating that – as ensembles – neurons can track extremely rapid input signals, varying in time much faster than single-cell output mean firing rate (<25 spikes/s in our experiments) and passive membrane filtering (~50 cycles/s).

Moreover, consistent with the definition of presynaptic inhibitory control of postsynaptic firing, when the input modulation $\Delta R_I(t)$ was applied only to the inhibitory presynaptic activation rate (see Fig. 3B-D, Fig. 5 third row), the output phase displayed an additional offset of $-\pi$, across all frequencies. In fact, the output rate reached its minimum when the input rate was maximal (*i.e.* maximally inhibiting the neuron), thus resulting in an *opposition of phase*. In addition, the phase always reached a peak at low values of *f* (insets of Fig. 5), corresponding to a phase advance described previously (Fuhrmann *et al.,* 2002; Köndgen *et al.,* 2008). For faster modulation frequencies, the phase quickly decreased (crossing zero, or the $-\pi$ offset, if present), substantially lagging behind the input. Beyond the cutoff frequency, graphically represented in Fig. 3A-B by vertical continuous lines, the phase linearly decreases as the product ($-\Delta t\, f$), reminiscent of the effect in the Fourier domain of a fixed time delay Δt (*i.e.* 1.08 ± 0.16 ms, range [1; 1.5], Fig. 5) (Fourcaud-Trocmé *et al.,* 2003; Köndgen *et al.,* 2008). For the sake of clarity, the same annotation labels and colour conventions used for Figs. 3-5 were used in Figs. 6-7 as well.

Output firing rate and synaptic background intensity affect neuronal transfer properties.

By adjusting the excitatory to inhibitory ratio by the parameter V_b in Eq. 4, we varied the output mean firing rate of the neuron and arbitrarily identified two levels of its activity: *low* (4–9 spike/s) and *high* (15–25 spike/s). As shown in the Supplemental Materials (Fig. S2) the *low* and *high* firing rate regimes are also naturally associated with *high* and *low* (coefficient of) variability of the interspike-intervals (distribution). Analogously, by increasing the average excitatory activation rate R_E from 7 kHz to 14 kHz (R_I as in Eq. 4), we tuned different intensities of the fluctuating synaptic conductances that we termed *weak* and *strong background* activity, respectively. The combination of mean firing rate (and CV) and background synaptic intensity thus define a total of four regimes that we considered when probing the neuronal dynamical response properties. Although, Figs. 4 and 5 already display (column-wise) the whole repertoire of data, in the following we describe and discuss the response magnitudes (Fig. 4) and plot them again after sorting as Figs. 6 and 7. Such a rearrangement of data visualization allows us to more clearly describe how the dynamical response properties are affected by the output mean firing rate or by the intensity of the background synaptic activity.

Regardless of quantitative differences induced by the input modulation protocol (i)-(iv), we found no effect of the output mean firing rate for very fast modulation frequencies, as shown in Fig. 6A–D. In this figure, results from 106 cells active at very similar (*low* or *high*) mean firing rates and receiving *strong* background synaptic activity (*i.e.* $R_{E0} = 14\ kHz$), were pooled together and summarized in each panel (A: n=14 cells at low rates, 12 at high rates; B: n=10 cells at low rates, 12 at high rates; C: n=17 cells at low rates, 12 at high rates; D: n=10 cells at low rates, 19 at high rates). In the figure, continuous lines are best-fit plots of the response of the phenomenological model, mentioned earlier and described in the Methods section, employed here particularly to offer a data-driven estimate of the cutoff frequency (vertical lines). Indeed, cutoff frequencies and power-law attenuation profile were barely affected, as apparent from comparison of the thick and thin continuous lines. However, for slow and intermediate input modulations, an increase in the mean firing rate and associated decrease in spiking variability reduce the transfer gain, shrinking the bandwidth and emphasizing a broad peak, located at ~100 cycle/s.

We next examined how the intensity of the background synaptic activity alters the neuronal dynamical response, and summarised in Figure 7 the comparison between regimes, focusing only on the low firing rate case. In this figure, results from 117 cells receiving very similar (*weak* or *strong*) background synaptic activity and firing at *low* mean firing rate, were pooled together and summarized in each (A: n=14 cells at strong, 19 at weak background activity; B: n=10 cells at strong, 16 at weak background activity; C: n=17 cells at strong, 20 at weak background activity; D: n=13 cells at strong, 8 at weak background activity).

The recreated background synaptic activity evidently shortened the cell effective time constant associated with membrane integration properties ($\tau = 8.4 \pm 2.8\ ms$ during weak background stimulation, compared to $\tau = 19.9 \pm 5\ ms$ at rest, $n = 81$ cells, $p < 10^{-10}$ and $\tau = 5.2 \pm 1.6\ ms$ during strong background stimulation, compared to $\tau = 20.4 \pm 5\ ms$ at rest, $n = 66$ cells, $p < 10^{-10}$; $p = 0.99$ for the comparison between the two groups of cells at rest, *i.e.* without background stimulation, two-sample Kolmogorov-Smirnov test). However, no effect was observed at very fast modulation frequencies and on the cutoff frequency of the response. On the other hand, increasing the intensity of background synaptic activity reduced the transfer gain for slow and intermediate modulations.

Taken together, all these results indicate that cortical pyramidal neurons overall behave like *band-pass* filters, with a bandwidth directly influenced both by the firing rate of the presynaptic population and by the output mean firing rate of the cell.

Bandwidth and spike onset rapidness. Previous theoretical studies have linked a neuron's bandwidth with the trajectory of its membrane voltage at the spike initiation (Fourcaud-Trocmé *et al.,* 2003; Ilin *et al.,* 2013). As mentioned previously, we best-fitted the parameters of a

phenomenological model to the population averages (shown as continuous lines in Figs. 3, 4, 6-7) and summarized their values in Tables 1 and 2 (corresponding to Figs. 6 and 7, respectively). The same best-fit procedure can be applied to each experiment (not shown) besides to the population averages, allowing us to extract for each individual cell, among other observables, the high frequency cutoff of the neuron's response in a completely data-driven manner.

Thus, we determined whether the value of such a cutoff correlated to any passive or active membrane properties of the cell, such as: membrane capacitance, input resistance, membrane time constant, AP half-width, maximal upstroke velocity, and specifically to AP onset rapidness as predicted. We found significant correlations when comparing cutoff with membrane capacitance ($r = 0.22$, $p < 10^{-2}$), input resistance ($r = -0.31$, $p < 10^{-4}$), APs' half width ($r = -0.27$, $p < 10^{-3}$) and maximal upstroke velocity ($r = 0.27$, $p < 10^{-2}$). In addition, we indeed found that the high frequency cutoff of each neuron strongly correlated with its AP onset rapidness ($r = 0.39$, $p < 10^{-3}$). This is demonstrated in Fig. 8, where each grey marker represents a cell and the red line is a linear fit to the data. These results, based on $n = 81$ cells, confirm the measurable influence of AP rapidness on the bandwidth of the dynamical response, a phenomenon analysed in theoretical studies (Fourcaud-Trocmé *et al.,* 2003; Ilin *et al.,* 2013) and anticipated by experimental work in human cortical neurons (Testa-Silva *et al.,* 2014).

Detection of abrupt input changes. In analogy to the current-clamp experiments performed by Tchumatchenko et al. (2011), we investigated how rapidly neurons can detect abrupt changes in their presynaptic input statistics. To this aim, we removed the sinusoidal oscillatory modulation of the instantaneous firing rate of the presynaptic excitatory population considered so far and replaced it by a step function, as detailed in Eq. 7 and sketched in Fig. 9A. This effectively caused a sudden imbalance in the excitation-inhibition ratio and led to a rapid increase in the output instantaneous firing rate, estimated by the peri-stimulus time histogram (PSTH) over thousands of trials. This is shown in Fig. 9B-C, where the responses to a 5% (left) or to a 10% (right) abrupt change in the presynaptic excitatory drive have been summarised over n=16 cells (*i.e.* n=8 per condition). In both cases, the settling time of the neuronal response was shorter than the average inter-spike interval (*i.e.* 200 ms at 5 spike/s) and the transient response displayed an overshoot. These features are consistent with the step-response of a band-pass transfer function (Fig. 4C, darker colours), particularly with the location of the cutoff frequency beyond 100 cycles/s. In fact, a band-pass filter is equivalent to the cascade of a low- and a high-pass filter, processing a step-changing waveform in series: intuitively, the former delays and smooths the step – as a sliding window integral – while the latter subsequently attenuates any remaining steady components of the response – as a differentiator, ultimately leading to an overshoot as observed in the PSTH. Surprisingly, when the stimulus was increased by 5% (but not 10%), we also observed a mild but significant transient decrease in the output instantaneous firing rate, lasting $\sim 2\ ms$ and immediately following the step change of the presynaptic rate (Fig. 7B).

To further quantify the neuronal responses, we applied the analysis proposed by Tchumatchenko et al. (2011) that assumes the existence of a downstream theoretical decoder that receives the spike trains of a (virtual) population of neurons. Of course, we always experimentally recorded one neuron at the time but, on a first approximation, we can swap time with ensemble averages and consider the N trials – collected for the same cell – as being representative of simultaneous observations from N (identical and independent) neurons. The decoder reports conventionally a detection of the step change in its input, only when the ensemble firing rate of the N neurons (*i.e.* the PSTH of Fig. 9B-C) falls outside the 95% confidence boundary, estimated on the distribution of firing rate observed before the step.

Upon subsequent calculation of the PSTH over increasing number of trials (*i.e.* N = 0 - 2000 "neurons") and bin size (*i.e.* detection windows 4-16 ms) and the conventional detection threshold, we were able to compute the probability of threshold crossing (Fig. 9D-G).

The decrease in the instantaneous firing rate, observed in the 5% condition, effectively delays the detection of the step (Figs. 9B–C). This is likely due to a combined effect of the fixed propagation delay Δt and of the biophysical properties of conductance-based inputs: a surge in presynaptic

excitation induces an effective depolarization of the membrane potential. As the driving force for inhibitory synaptic conductances increases for increasing depolarizations, this in turn leads to a decrease in overall firing rate, at least immediately after the stimulation onset. After this initial phase, the postsynaptic firing rate increased in both cases, leading to the efficient and fast detection of the step-change (Figs. 9D-E): as expected, the steepness of the increase in detection probability as a function of time since the step grows with the number of postsynaptic neurons considered. We also calculated the probability of step detection as a function of the number of neurons across several delay times (Tchumatchenko *et al.,* 2011), ranging from 4 to 16 ms (Figs. 9F-G).

Taken together, our results demonstrate that – as ensembles – neurons can detect subtle changes in their inputs with reaction times much faster than intrinsic membrane properties and mean inter-spike intervals. Compared to previous results obtained in current clamp experiments (Tchumatchenko *et al.,* 2011), our experiments show how the detection of an increase in presynaptic firing rate may be slightly delayed if its magnitude is small compared to the baseline presynaptic firing rate.

Discussion

We are the first group to investigate the properties of dynamical transfer of fast time-varying input signals by cortical ensembles in a biophysically realistic *in vitro* setting. We recreated fluctuating conductance-driven background synaptic activity by dynamic-clamp, balancing excitation and inhibition, and applied foreground small-amplitude stimuli as current- or conductance-driven waveforms across a broad range of experimental conditions. We were particularly interested in how neuronal responses are affected by the type of input modulation (*i.e.* current- or conductance-based), the intensity of the recreated synaptic background, and the output firing rate of the neurons, consistently with previous works and findings (Köndgen *et al.,* 2008; Broicher *et al.,* 2012; Litwin-Kumar *et al.,* 2011). Our results extend previous observations and show that no qualitative differences exist in transferring time-varying information encoded as conductance or current inputs.

The impact of the modulation type on dynamical responses was previously explored theoretically in integrate-and-fire (IF) models (Richardson, 2007). Upon an effective rescaling of the membrane time constant induced by conductance fluctuations, conductance and current stimuli lead to quantitative and not qualitative differences in IF models. Then a higher intensity of the recreated synaptic background would further increase the membrane time constant and alter the cutoff frequency. In our conductance-clamp experiments however, despite a reduction up to 60-75% of the effective membrane time constant compared to rest, we observed almost no difference with current-clamp data (Köndgen *et al.*, 2008) and particularly no change in the cutoff and attenuation of very fast modulations. In addition, we found no clear effect of the output mean firing rate on the cutoff frequency, as described in numerous studies (Fourcaud-Trocmé *et al.,* 2003). It is possible that these differences may be reconciled by choosing different numerical values of IF model parameters (*e.g.* the sharpness of action potentials in non-linear integrate-and-fire model neurons much larger than measured directly) to be interpreted only as indirect correlates of biophysical observables.

In all cases studied experimentally, we found that neurons display a band-pass behaviour with very large cutoff frequencies (~200–400 cycles/s), comparable across all conditions. For very fast input modulations, neurons attenuated their inputs by a power law with negative exponents in the range [-1.5; -0.9] as previously reported (Köndgen *et al.,* 2008) and reminiscent of an effective non-linearity of spike initiation in IFs, which is intermediate between exponential and quadratic (Richardson, 2007; Fourcaud-Trocmé and Brunel, 2005).

For slow and intermediate modulations, the gain of the dynamical response appears in direct relationship with the variability of inter-spike intervals and to its mean (*i.e.* in inverse relationship with the output firing rate, as shown in Fig. 6). This might be attributable to spike-rate adaptation, due to its known higher reduction of the slope of the (stationary) F–I curve at higher firing rates as well as its associated high-pass dynamical behaviour (Fuhrmann *et al.,* 2002) in cascade to neuronal intrinsic filtering. In fact, the spike-rate adaptation depends on the accumulation of intracellular free sodium, free calcium or on alternative negative-feedback state variables with marked temporal integrative properties of the firing rate (Koch, 1998). It follows that these variables cannot track very

fast changes of the firing rate over time, thus constraining their effect for slow modulations. However, there are known alternative mechanisms to account for high-pass dynamical behaviours or resonances, such as morphology (Ostojic *et al.,* 2015) or subthreshold membrane properties (Brunel *et al.,* 2003).

Cortical neurons *in vivo* are more depolarized and have lower input resistance than *in vitro*, while membrane voltage dynamics are dominated by irregular firing and subthreshold fluctuations in the range of 3–5 mV (Destexhe *et al.,* 2003; Ho and Destexhe, 2000). These conditions, and in particular the higher variability of the inter spike interval, might favour a broadening of the pass-band profile of the transfer function while leaving its overall magnitude and cutoff unaffected.

We then considered an earlier study where the background synaptic activity was shown experimentally to modulate the slope of the (stationary) F–I curve (Chance *et al.,* 2002). The conclusions of that study are now generalised as follows: the intensity of the background of excitatory and inhibitory synaptic inputs within active cortical circuits acts as a modulatory signal, but the extent of its control on cell dynamical transfer properties occurs exclusively for slowly changing inputs, allowing rapidly changing inputs to be relayed downstream unaffected (Fig. 7). We also remark that, despite a significant reduction of the effective membrane time constant, no change in the cutoff frequency or high-frequency behaviour of the dynamical response was observed.

In addition, our data support unambiguously the correlation between the cutoff frequency of individual neurons and the rapidness of their spike onset dynamics, in qualitative agreement with theoretical predictions (Brunel and Wang, 2003; Fourcaud-Trocmé and Brunel, 2005; Naundorf *et al.,* 2006; Ilin *et al.,* 2013) and with an experimental comparative work (Testa-Silva *et al.,* 2014). We have evidence, to be discussed elsewhere in detail, that the quantitative features of the dynamical transfer properties are reproduced *in silico* by multicompartmental (Markram *et al.,* 2015) but not single-compartmental model neurons (Fourcaud-Trocmé *et al.,* 2013). Anatomically and physiologically detailed model neurons, algorithmically fitted on independent experimental data (Ramaswamy *et al.,* 2015), display cutoff frequencies of ~200–400 cycles/s without parameter adjustments (data not shown). As these models include conventional gating of sodium channels and detailed reconstructions of the dendritic but not of the axonal trees, only the electrotonic dendritic load (Eyal *et al.,* 2014) and critical resistive coupling theories (Brette, 2013), but neither channel gating cooperativity (Naundorf *et al.,* 2006; Ilin *et al.,* 2013) nor AP backpropagation from the axon (McCormick *et al.,* 2007; Yu *et al.,* 2008) seem necessary for rapid somatic AP onset and broad dynamical bandwidth.

Finally, we sought to investigate the rapidness by which neuronal ensembles can detect abrupt increases in the firing rate of their presynaptic partners. We found that, despite the rapidness of the neuronal response and in contrast to current-clamp inputs (Tchumatchenko *et al.,* 2011) a step-like increase in the excitatory presynaptic firing rate $\Delta R_E(t)$ produces a small but noticeable decrease in the output firing rate when the increase in presynaptic excitatory firing rate is small compared to the baseline. This constitutes a lower limit to the speed by which changes in the input statistics can be reliably detected by a large population of postsynaptic neurons.

In summary, our systematic study on the input–output dynamical response properties of cortical neurons confirms and generalizes previous theoretical and experimental works. It further offers the experimental and computational research communities a novel tool to classify and probe intrinsic neuronal properties, and constrain the realism of reduced mathematical models of excitability and information integration (Brette, 2015). This is important for the advancement of our understanding of the biophysical mechanisms underlying fast computations in cortical ensembles, as well as for the emergence of network-driven oscillations in recurrent microcircuitry.

Acknowledgements

We are grateful to Mr. D. Van Dyck and M. Wijnants for excellent technical assistance, to Drs. J. Couto, M. Negrello, M.J.E. Richardson, A. Neef, P. Vanderhaeghen for helpful discussions, to the anonymous referees and Dr. B. Martin for improving the quality of the manuscript. Financial support from the European Commission (FP7-ICT-FET project "BRAINLEAP", grant n. 306502; H2020-

ICT-FET-FLAGSHIP "Human Brain Project" – SGA1, grant n. 720270), the Interuniversity Attraction Poles Program "Phase VII" of the Belgian Science Policy Office, and the Flemish Research Foundation (grant n. G0F1517N) is kindly acknowledged.

References

Abbott, L.F. & Chance, F.S. (2005) Drivers and modulators from push-pull and balanced synaptic input. *Prog. Brain. Res.*, **149**,147-155.

Arsiero, M., Lüscher, H.R., Lundstrom, B.N. & Giugliano, M. (2007) The impact of input fluctuations on the frequency-current relationships of layer 5 pyramidal neurons in the rat medial prefrontal cortex. *J. Neurosci.*, **27**(12), 3274-3284.

Bal, T. & Destexhe, A. (2009) *Dynamic-clamp: From principles to applications*. Springer, New York.

Biró, I. & Giugliano, M. (2015) A reconfigurable visual-programming library for real-time closed-loop cellular electrophysiology. *Front. Neuroinform.*, **9**, 17.

Brette, R. (2015) What Is the Most Realistic Single-Compartment Model of Spike Initiation? *PLoS Comput. Biol.*, **11**(4), e1004114.

Brette, R., Piwkowska, Z., Monier, C., Rudolph-Lilith M., Fournier, J., Levy, M., Fregnac, Y., Bal, T. & Destexhe, A. (2008) High-resolution intracellular recordings using a real-time computational model of the electrode. *Neuron*, **59**, 379-391.

Brette, R., (2013) Sharpness of Spike Initiation in Neurons Explained by Compartmentalization. *PLoS Comput. Biol.*, **9**(12), e1003338.

Broicher, T., Malerba, P., Dorval A.D., Borisyuk, A., Fernandez, F.R. & White, J.A. (2012) Spike phase locking in CA1 pyramidal neurons depends on background conductance and firing rate. *J. Neurosci.*, **32**, 14374-14388.

Brunel, N., Chance, F.S., Fourcaud, N. & Abbott, L. (2001) Effects of synaptic noise and filtering on the frequency response of spiking neurons. *Phys. Rev. Lett.,* **86**(10), 2186-2189.

Brunel, N., Hakim, V. & Richardson, M. (2003) Firing-rate resonance in a generalized integrate-and-fire neuron with subthreshold resonance. *Phys. Rev. E*, **67**(5), 051916.

Brunel, N. & Wang, X.J. (2003) What determines the frequency of fast network oscillations with irregular neural discharges? I. synaptic dynamics and excitation-inhibition balance. *J. Neurophysiol.*, **90**, 415-430.

Boucsein, C., Tetzlaff, T., Meier, R., Aertsen, A. & Naundorf, B. (2009) Dynamical response properties of neocortical neuron ensembles: multiplicative versus additive noise. *J. Neurosci.*, **29**(4), 1006-1010.

Buzsaki, G. & Draguhn, A. (2004) Neuronal oscillations in cortical networks. *Science*, **304**, 1926-1929.

Chance, F.S., Abbott, L.F. & Reyes, A.D. (2002) Gain modulation from background synaptic input. *Neuron*, **35**, 773-782.

Destexhe, A. (2010) Inhibitory "noise". *Front. Cell. Neurosci.*, **4**, 9.

Destexhe, A., Rudolph, M. & Pare, D. (2003) The high-conductance state of neocortical neurons in vivo. *Nat. Rev. Neurosci.*, **4**, 739-751.

Destexhe, A., Rudolph, M., Fellous, J.M. & Sejnowski, T.J. (2001) Fluctuating synaptic conductances recreate in vivo-like activity in neocortical neurons. *Neuroscience*, **107**, 13-24.

Economo, M.N., Fernandez, F.R. & White, J.A. (2010) Dynamic clamp: Alteration of response properties and creation of virtual realities in neurophysiology. *J. Neurosci.*, 30, 2407-2413.

Eyal, G., Mansvelder, H.D., de Kock, C.P. & Segev, I. (2014) Dendrites impact the encoding capabilities of the axon. *J. Neurosci.*, **34**(24), 8063-71.

Fourcaud-Trocmé, N. & Brunel, N. (2005) Dynamics of the instantaneous firing rate in response to changes in input statistics. *J. Comput. Neurosci.*, **18**, 311-321.

Fourcaud-Trocmé, N., Hansel, D., van Vreeswijk, C. & Brunel, N. (2003) How spike generation mechanisms determine the neuronal response to fluctuating inputs. *J. Neurosci.*, **23**, 11628-11640.

Fuhrmann, G., Markram, H. & Tsodyks, M. (2002) Spike frequency adaptation and neocortical rhythms. *J. Neurophysiol.*, *88*(2), 761-770.

Geisler, C., Brunel, N. & Wang, X.J. (2005) Contributions of intrinsic membrane dynamics to fast network oscillations with irregular neuronal discharges. *J. Neurophysiol.*, **94**(6), 4344-4361.

Giugliano, M., La Camera, G., Fusi, S. & Senn, W. (2008) The response of cortical neurons to in vivo-like input current: Theory and experiment: II. time-varying and spatially distributed inputs. *Biol. Cybern.*, **99**, 303-318.

Henze, D.A., Buzsaki, G. (2001) Action potential threshold of hippocampal pyramidal cells in vivo is increased by recent spiking activity. *Neuroscience*, **105**, 121-130.

Ho, N., Destexhe, A. (2000) Synaptic background activity enhances the responsiveness of neocortical pyramidal neurons. *J. Neurophysiol*., **84**, 1488-1496.

Ilin, V., Malyshev, A., Wolf, F. & Volgushev, M. (2013) Fast computations in cortical ensembles require rapid initiation of action potentials. *J. Neurosci.*, **33**, 2281-2292.

Koch, C. (1998) *Biophysics of computation: information processing in single neurons*. Oxford University Press, New York.

Köndgen, H., Geisler, C., Fusi, S., Wang, X.J., Lüscher, H.R. & Giugliano, M. (2008) The dynamical response properties of neocortical neurons to temporally modulated noisy inputs in vitro. *Cereb. Cor.*, **18**, 2086-2097.

La Camera, G., Senn, W. & Fusi, S. (2004) Comparison between networks of conductance-and current-driven neurons: stationary spike rates and subthreshold depolarization. *Neurocomputing*, **58**, 253-8.

La Camera, G., Giugliano, M., Senn, W. & Fusi, S. (2008) The response of cortical neurons to in vivo-like input current: theory and experiment: I. Noisy inputs with stationary statistics. *Biol. Cybern.*, **99**(4-5), 279-301.

Linaro, D., Couto, J. & Giugliano, M. (2014) Command-line cellular electrophysiology for conventional and real-time closed-loop experiments. *J. Neurosci. Meth.*, **230**, 5-19.

Litwin-Kumar, A., Oswald, A.M., Urban, N.N. & Doiron, B. (2011) Balanced synaptic input shapes the correlation between neural spike trains. *PLoS Comput. Biol*., **7**, e1002305.

Markram, H., Muller, E., Ramaswamy, S., Reimann, M.W., Abdellah, M., Sanchez, C.A., Ailamaki, A., Alonso-Nanclares, L., Antille, N., Arsever, S., Kahou, G.A.A., Berger, T.K., Bilgili, A., Buncic, N., Chalimourda, A., Chindemi, G., Courcol, J.D., Delalondre, F., Delattre, V., Druckmann, S., Dumusc, R., Dynes, J., Eilemann, S., Gal, E., Gevaert, M.E., Ghobril, J.P., Gidon, A., Graham, J.W., Gupta, A., Haenel, V., Hay, E., Heinis, T., Hernando, J.B., Hines, M., Kanari, L., Keller, D., Kenyon, J., Khazen, G., Kim, Y., King, J.G., Kisvarday, Z., Kumbhar, P., Lasserre, S., Le Bé, J.V., Magalhães, B.R.C., Merchán-Pérez, A., Meystre, J., Morrice, B.R., Muller, J., Muñoz-Céspedes, A., Muralidhar, S., Muthurasa, K., Nachbaur, D., Newton, T.H., Nolte, M., Ovcharenko, A., Palacios, J., Pastor, L., Perin, R., Ranjan, R., Riachi, I., Rodríguez, J.R., Riquelme, J.L., Rössert, C., Sfyrakis, K., Shi, Y., Shillcock, J.C., Silberberg, G., Silva, R., Tauheed, F., Telefont, M., Toledo-Rodriguez, M., Tränkler, T., Van Geit, W., Díaz, J.V., Walker, R., Wang, Y., Zaninetta, S.M., DeFelipe, J., Hill, S.L., Segev, I. & Schürmann, F. (2015) Reconstruction and Simulation of Neocortical Microcircuitry. *Cell*, **163**, 2, 456-492.

McCormick, D.A., Connors, B.W., Lighthall, J.W. & Prince, D.A. (1985) Comparative electrophysiology of pyramidal and sparsely spiny stellate neurons of the neocortex. *J. Neurophysiol.*, **54**, 782-806.

McCormick, D.A., Shu, Y. & Yu, Y. (2007) Hodgkin and Huxley model still standing? *Nature*, **445**, E1-E2.

Naundorf, B., Wolf, F. & Volgushev, M. (2006) Unique features of action potential initiation in cortical neurons. *Nature*, **440**(7087), 1060-1063.

Naundorf, B., Geisel, T. & Wolf, F. (2005) Action potential onset dynamics and the response speed of neuronal populations. *J. Comp. Neurosci.*, **18**, 297-309.

Ostojic, S., Szapiro, G., Schwartz, E., Barbour, B., Brunel, N. & Hakim, V. (2015) Neuronal morphology generates high-frequency firing resonance. *J. Neurosci.*, **35**, 7056-7068.

Ramaswamy, S., Courcol, J.D., Abdellah, M., Adaszewski, S.R., Antille, N., Arsever, S., Atenekeng, G., Bilgili, A., Brukau, Y., Chalimourda, A., Chindemi, G., Delalondre, F., Dumusc, R., Eilemann, S., Gevaert, M.E., Gleeson, P., Graham, J.W., Hernando, J.B., Kanari, L., Katkov, Y., Keller, D., King, J.G., Ranjan, R., Reimann, M.W., Rössert, C., Shi, Y., Shillcock, J.C,. Telefont, M., Van Geit, W., Villafranca Diaz, J., Walker, R., Wang, Y., Zaninetta, S.M., DeFelipe, J., Hill, S.L., Muller, J., Segev, I., Schürmann, F., Muller, E.B. & Markram, H. (2015) The Neocortical Microcircuit Collaboration Portal: A Resource for Rat Somatosensory Cortex. *Front. Neural Circuits*, **9**, 44.

Richardson, M.J.E. (2007) Firing-rate response of linear and nonlinear integrate-and-fire neurons to modulated current-based and conductance-based synaptic drive. *Phys. Rev. E*, **76**, 021919.

Robinson, H.P. & Kawai, N. (1993) Injection of digitally synthesized synaptic conductance transients to measure the integrative properties of neurons. *J. Neurosci. Meth.*, **49**, 157-165.

Sceniak, M.P. & Sabo, S.L. (2010) Modulation of firing rate by background synaptic noise statistics in rat visual cortical neurons. *J. Neurophysiol.*, **104**, 2792-2805.

Silberberg, G., Bethge, M., Markram, H., Pawelzik, K. & Tsodyks, M. (2004) Dynamics of population rate codes in ensembles of neocortical neurons. *J. Neurophysiol.*, *91*(2), 704-709.

Testa-Silva, G., Verhoog, M.B., Linaro, D., de Kock, C.P.J., Baayen, J.C., Meredith, R.M., Rhiannon M. Meredith, De Zeeuw, C.I., Giugliano, M. & Mansvelder, H.D. (2014) High bandwidth synaptic communication and frequency tracking in human neocortex. *PLoS Biol.*, **12**(11), e1002007.

Tiesinga, P.H., José, J.V. & Sejnowski, T.J. (2000) Comparison of current-driven and conductance-driven neocortical model neurons with Hodgkin-Huxley voltage-gated channels. *Phys. Rev. E*, ***62***(6 Pt B), 8413-8419.

Tchumatchenko, T., Malyshev, A., Wolf, F. & Volgushev, M. (2011) Ultrafast population encoding by cortical neurons. *J. Neurosci.*, **31**(34), 12171-12179.

Uhlenbeck, G.E. & Ornstein, L.S. (1930) On the theory of the brownian motion. *Phys. Rev*., **36**, 823-841.

Wang, X.-J. (2010) Neurophysiological and computational principles of cortical rhythms in cognition. *Physiol. Rev.*, **90**(3), 1195-1268.

Wei, W. & Wolf, F. (2011) Spike onset dynamics and response speed in neuronal populations. *Phys. Rev. Lett.*, **106**, 088102.

Yu, Y., Shu, Y. & McCormick, D.A. (2008) Cortical action potential backpropagation explains spike threshold variability and rapid-onset kinetics. *J. Neurosci.*, **28**, 7260-7272.

Tables

Input Modulation	Firing rate	Synaptic background	A	z_1 (Hz)	p_1 (Hz)	p_2 (Hz)	p_3 (Hz)	Δt (ms)
ΔI	*Low*	*Strong*	0.2097	3.94	10.4	490.9	490.9	0.87
ΔI	*High*	*Strong*	0.1043	4.94	35.0	456.7	456.7	1.04
ΔR_E & ΔR_I	*Low*	*Strong*	0.1101	2.40	10.4	363.3	663.5	1.08
ΔR_E & ΔR_I	*High*	*Strong*	0.0784	4.88	38.9	460.7	460.7	1.12
ΔR_E	*Low*	*Strong*	0.2139	3.49	9.1	448.3	448.3	1.36
ΔR_E	*High*	*Strong*	0.0565	7.79	252.6	252.6	252.6	0.90
ΔR_I	*Low*	*Strong*	0.4295	3.78	8.95	550.6	550.6	1.10
ΔR_I	*High*	*Strong*	0.1013	3.28	41.2	467.1	467.1	1.16

Table 1: The experimental data (markers) of Figure 6 were compared to the response of a linear filter model (Eq. 9 – continuous lines in Fig. 6), with 6 free parameters. The values in the table are the best-fit parameters to account for magnitude (normalised to the mean) and phase of the response simultaneously.

Input Modulation	Firing rate	Synaptic background	A	z_1 (Hz)	p_1 (Hz)	p_2 (Hz)	p_3 (Hz)	Δt (ms)
ΔI	*Low*	*Strong*	0.2097	3.94	10.4	490.9	490.9	0.87
ΔI	*Low*	*Weak*	0.2352	2.55	5.8	593.1	593.1	0.87
ΔR_E & ΔR_I	*Low*	*Strong*	0.1101	2.40	10.4	363.3	663.5	1.08
ΔR_E & ΔR_I	*Low*	*Weak*	0.2021	2.26	5.7	337.1	542.0	1.02
ΔR_E	*Low*	*Strong*	0.2139	3.49	9.1	448.3	448.3	1.36
ΔR_E	*Low*	*Weak*	0.2777	1.02	2.5	361.6	361.6	1.32
ΔR_I	*Low*	*Strong*	0.4295	3.78	8.95	550.6	550.6	1.10
ΔR_I	*Low*	*Weak*	0.4512	1.59	3.9	481.9	481.9	1.08

Table 2: The experimental data (markers) of Figure 7 were compared to the response of a linear filter model (Eq. 9 – continuous lines in Fig. 7), with 6 free parameters. The values in the table are the best-fit parameters to account for the magnitude (normalised to the mean) and phase of the response simultaneously.

Figures and Figure captions

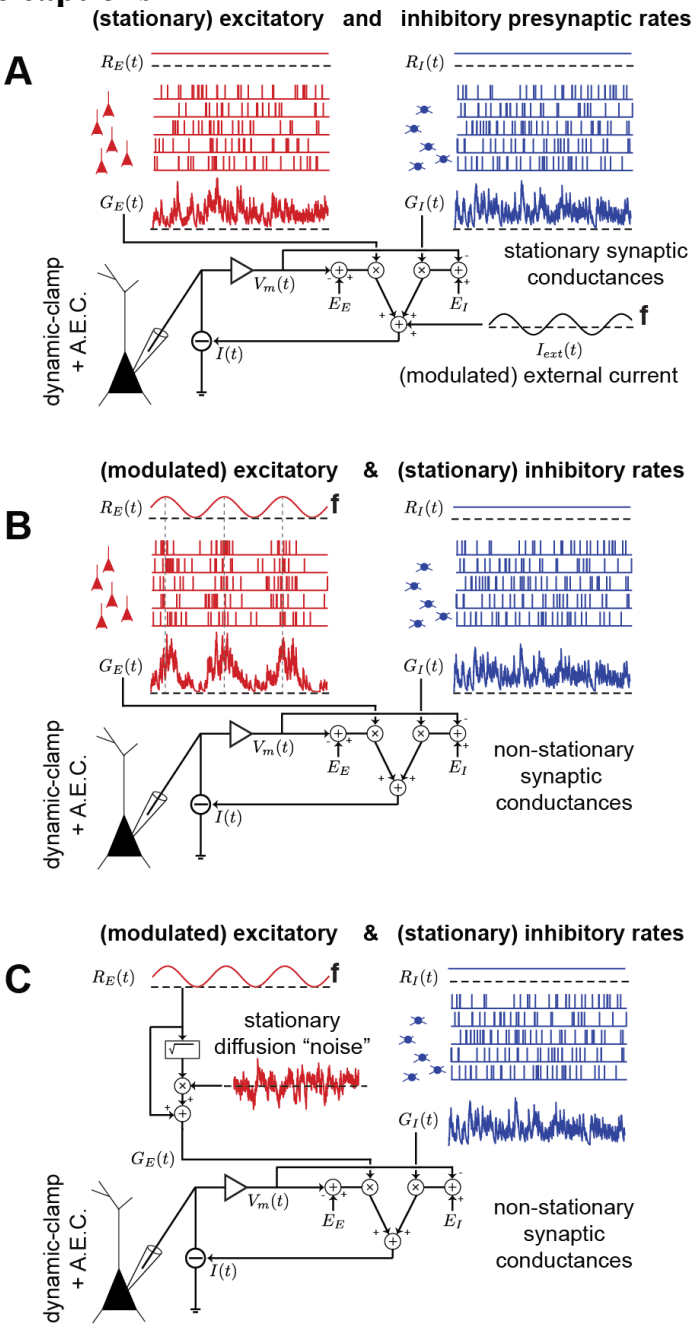

Figure 1: **The dynamics of neuronal responses was investigated upon injection of time-varying recreated synaptic inputs.** Dynamic-clamp with active electrode compensation (A.E.C.) recreates the effects of *in vivo*-like activation of presynaptic afferents. We investigated the cell firing in response to a sinusoidal input with frequency *f*, applied (**A**) as an external current $I_{ext}(t)$, (**B**) as a modulation of either excitatory $R_E(t)$ or inhibitory $R_I(t)$ presynaptic afferent rates, or both (not represented). Despite (**B**)'s higher biophysical realism than (**A**), injected synaptic conductances (*e.g.* $G_E(t)$) displayed significant attenuation and phase lag for fast input modulations. Such a "low-pass" filtering is solely due to the kinetics of the synthetic synapses, it reduces the signal-to-noise ratio of the cell response, but (**C**) can be compensated for while leaving the spectral properties of synaptic fluctuations unaltered.

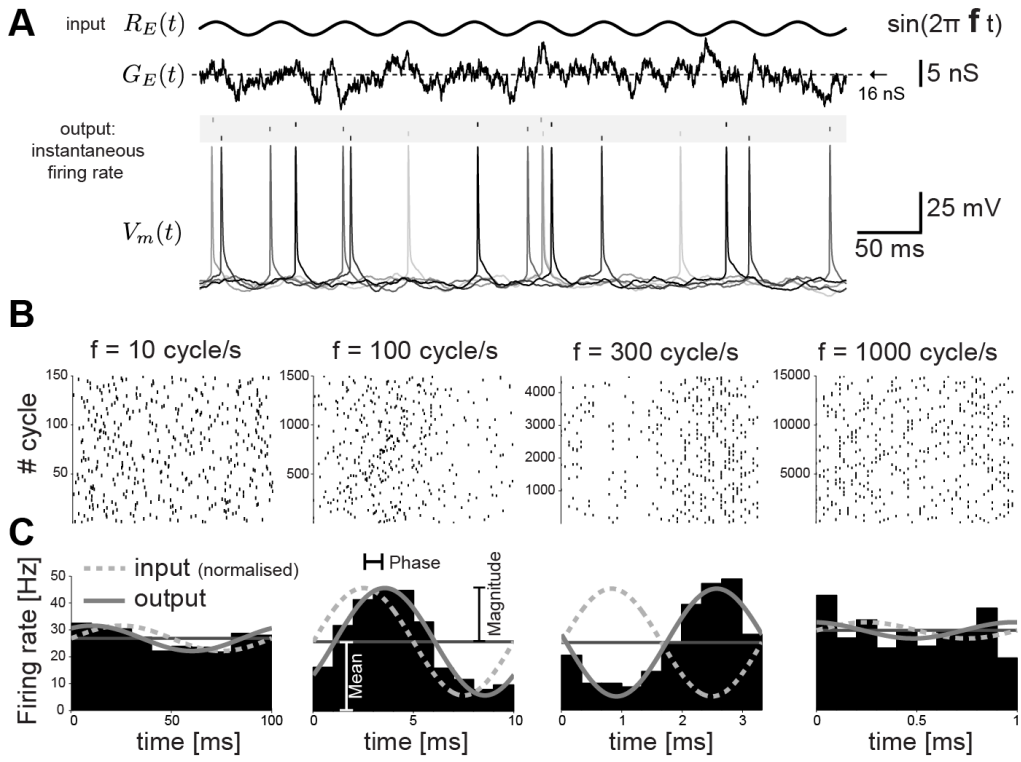

Figure 2: **Neuronal instantaneous output firing rates track fast modulations of synaptic inputs.** Exemplifying one of the stimulation protocols, a realization of the conductance $G_E(t)$ is shown (**A**, upper trace): its mean and variance follow the sinusoidal modulation of the input presynaptic rate $R_E(t)$. In response to it, the neuron fires sparsely (**A**, lower trace) but its instantaneous firing rate - estimated across input cycles and repetitions (**B**) as the peri-stimulus spike times histogram (PSTH - **C**) - reveal output temporal modulations. These occur at the same frequency *f* of the input (up to *300 cycle/s*) and are quantified in terms of mean, magnitude, and phase, as depicted in **C**. Note that both magnitude and phase depend on *f*.

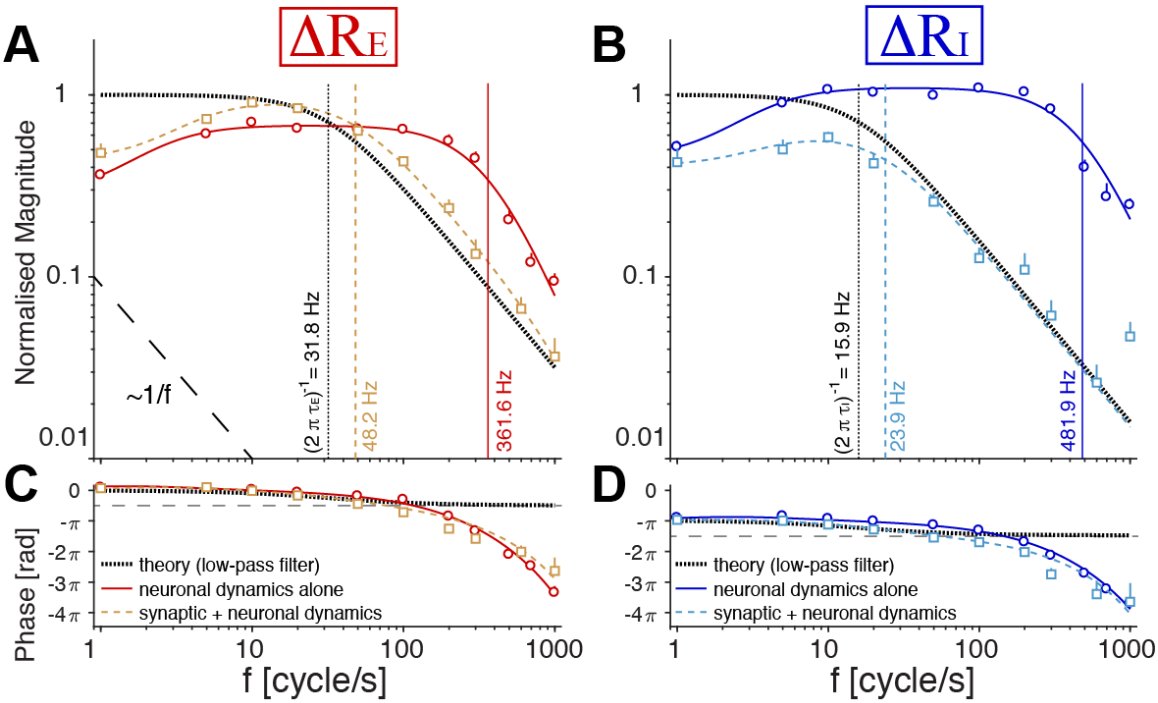

Figure 3: Accurately probing neurons' dynamical response to fast modulations by compensating for the (recreated) synaptic filtering. We used alternatively two stimulation

protocols that induce filtered (square markers) or instantaneous (circular markers) oscillations in the injected synaptic conductances. Magnitude (**A**-**B**; normalised to its mean) and phase (**C**-**D**) of the output instantaneous firing rate are displayed over a wide range of *f*, upon modulating the excitatory $R_E(t)$ (**A**, **C**) or inhibitory $R_I(t)$ (**B**, **D**) presynaptic input rates. Circular markers indicate the population transfer function in response to the injection of instantaneously-modulated conductances, while square markers refer to the transfer function filtered by the transfer properties of synthetic synapses (dotted black lines, in all panels). Solid thin (dashed and continuous) lines are optimal fits of a phenomenological model whose cutoff frequencies are indicated by the vertical lines. The black dashed line in (**A**) indicates the ~1/f slope.

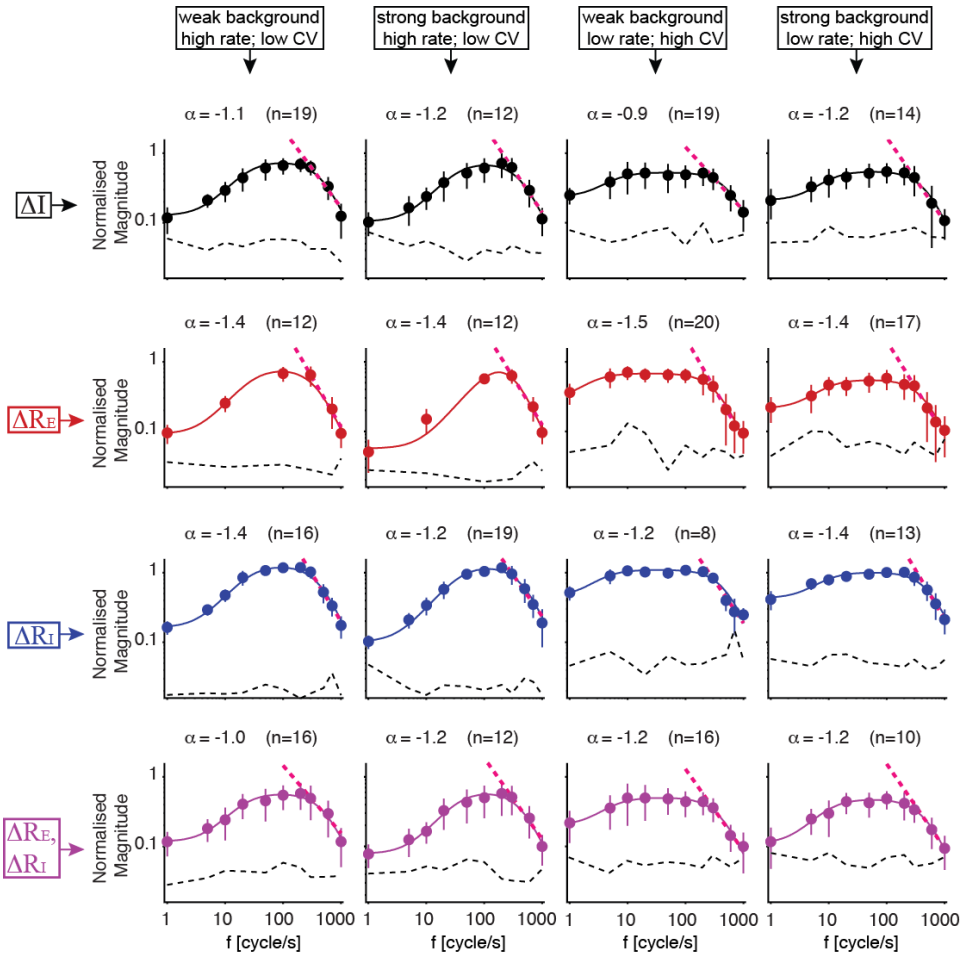

Figure 4: Across firing regimes and stimulation protocols, the neuronal gain reveals similar characteristic features: high *cutoff* frequency, broad band-pass profile, and power-law attenuation at very fast modulations. Each panel displays the magnitude (normalised to its mean) of the output instantaneous firing rate as a function of *f* across distinct physiological regimes (column-wise). Row-wise, input sinusoidal modulations were delivered as an external current amplitude, as both excitatory $R_E(t)$ and inhibitory $R_I(t)$ presynaptic input rates simultaneously, or only one of them at the time. Markers are the magnitude of the population transfer function in response to the injection of instantaneously-modulated conductances. The solid lines are optimal fits of a phenomenological model (see the Methods), the red dashed lines are best fits of f^{α}. The black dashed curves represent data-driven response minimal significance thresholds. For each panel, the number of cells and the estimated parameter α are indicated.

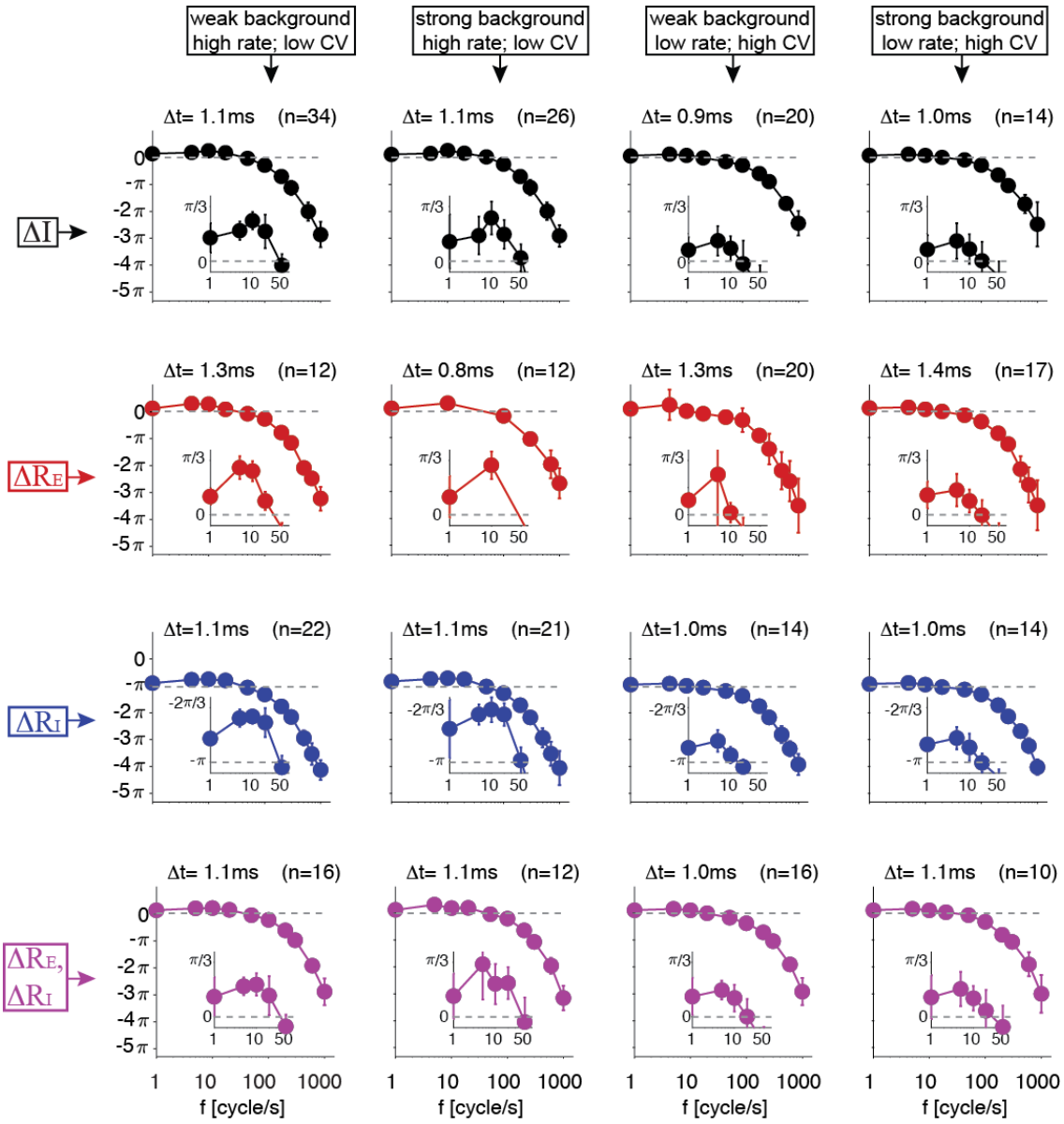

Figure 5: Across firing regimes and stimulation protocols, the phase of neuronal response reveals similar characteristic features: phase-advance for slow modulations, phase lag at intermediate and fast modulations, and a linear increase ~ *-f Δt* at very fast modulations. Each panel displays the phase (referred to the input sine) of the output instantaneous firing rate as a function of *f*, across distinct physiological regimes (column-wise). Row-wise, input sinusoidal modulations were delivered as an external current amplitude, as both excitatory $R_E(t)$ and inhibitory $R_I(t)$ presynaptic input rates simultaneously, or only one of them at the time. Markers indicate the phase of the population transfer function in response to the injection of instantaneously-modulated conductances. The grey dashed lines represent 0 and -π. For each panel, the number of cells and the estimated parameter *Δt* are indicated.

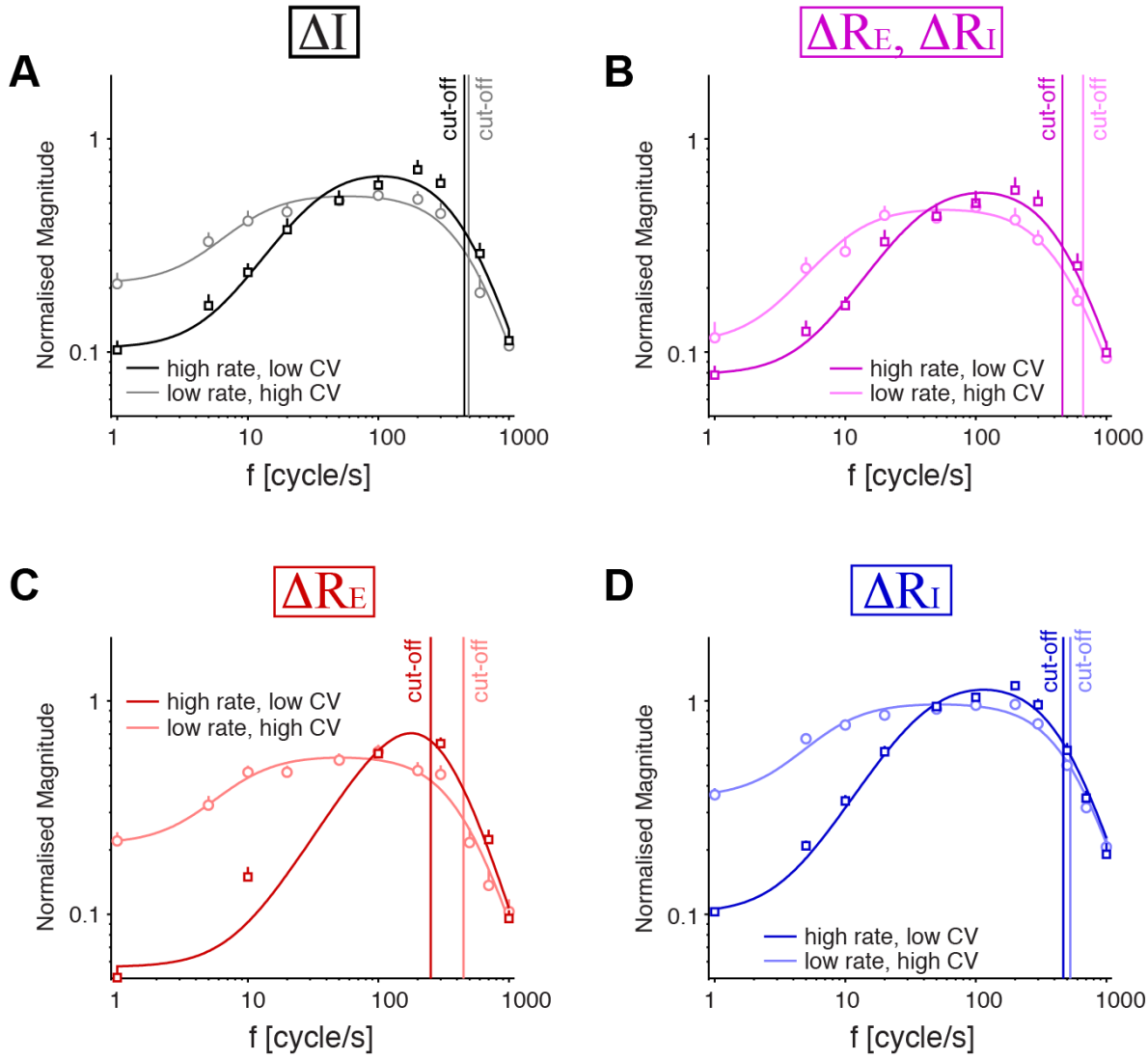

Figure 6: Increasing the output mean firing rate leaves the *cutoff* of neuronal gain unaltered, and attenuates the transfer of slow but not fast input modulations. Each panel displays the magnitude (normalised to its mean) of the output instantaneous firing rate as a function of f, under strong background fluctuations, while modulating an external current amplitude (**A**), both excitatory $R_E(t)$ and inhibitory $R_I(t)$ presynaptic input rates simultaneously (**B**), or only one of them at the time (**C**, **D**). Circular (square) markers are the magnitude of the population transfer function in response to the injection of instantaneously-modulated conductances, at low (high) output mean firing rates. The solid lines are optimal fits of a phenomenological model (see the Methods) and the vertical lines indicate its cutoff frequency.

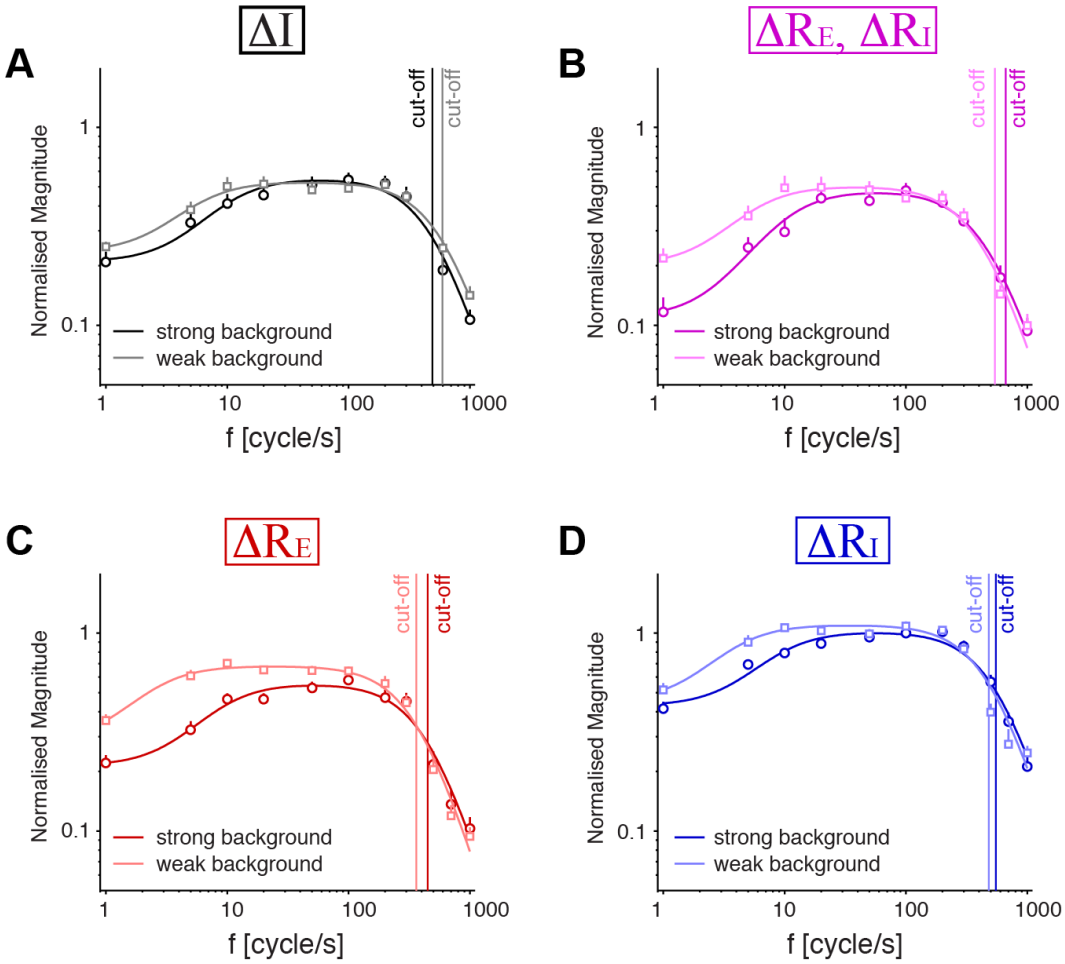

Figure 7: Increasing the synaptic background intensity leaves the *cutoff* and the *bandwidth* of neuronal gain unaltered, and attenuates the transfer of slow but not fast input modulations. Each panel displays the magnitude (normalised to its mean) of the output instantaneous firing rate as a function of f at low output mean firing rates, while modulating an external current amplitude (**A**), both excitatory $R_E(t)$ and inhibitory $R_I(t)$ presynaptic input rates simultaneously (**B**), or only one of them at the time (**C**, **D**). Square (circle) markers are the magnitude of the population transfer function in response to the injection of instantaneously-modulated conductances, under weak (strong) intensity of background synaptic fluctuations. The solid lines are optimal fits of a phenomenological model and the vertical lines indicate its cutoff frequency.

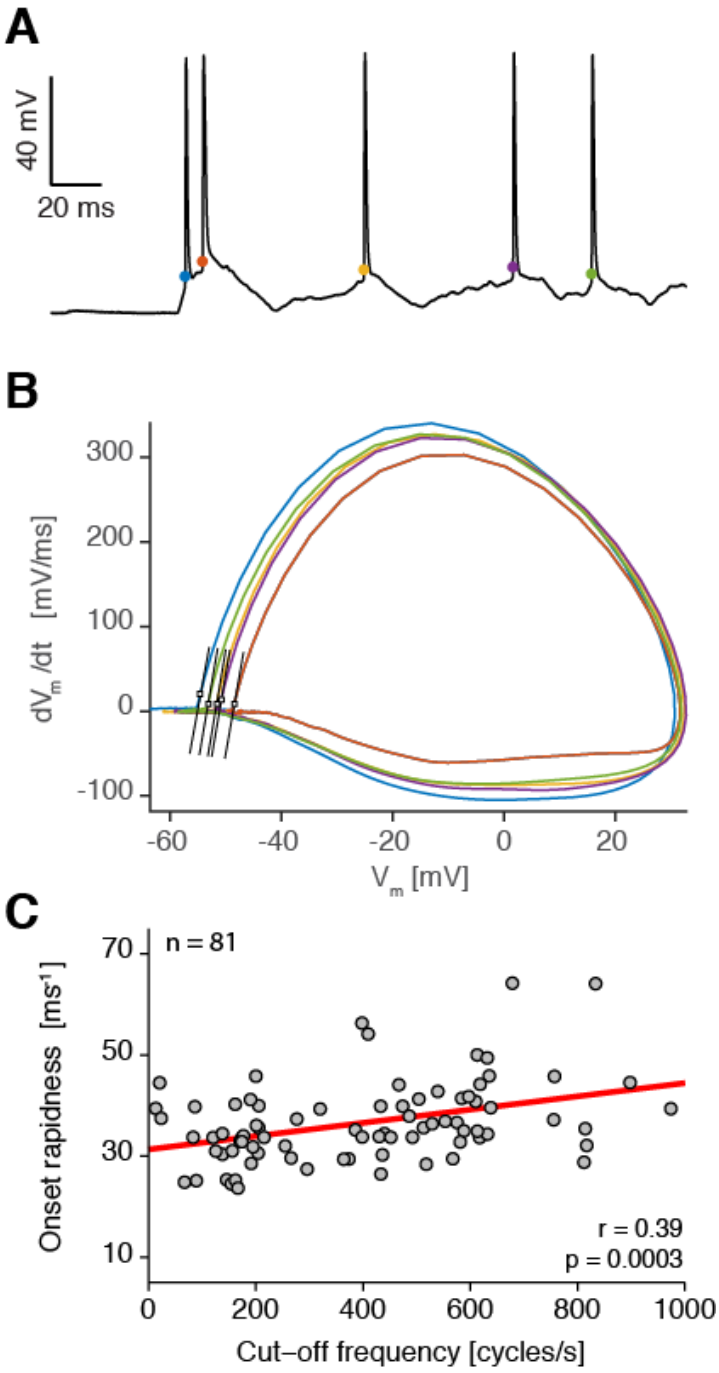

Figure 8: The "bandwidth" of neuronal gain is significantly correlated with the action potentials' (AP) rapidness at their onset. For each AP in a sample membrane voltage trace (**A**), its onset voltage is highlighted as a dot. When represented in the plane V_m *versus* $\mathrm{d}V_m/\mathrm{d}t$, each AP is a closed trajectory and its rapidness conventionally expressed as the slope of the trace at the onset voltage (**B**). For each of 81 cells, average AP onset rapidness was correlated and plotted *versus* the gain cutoff frequency for the same cell: a significant (Person's) correlation is revealed. Markers represent individual cells, while the red line is a linear fit to the data.

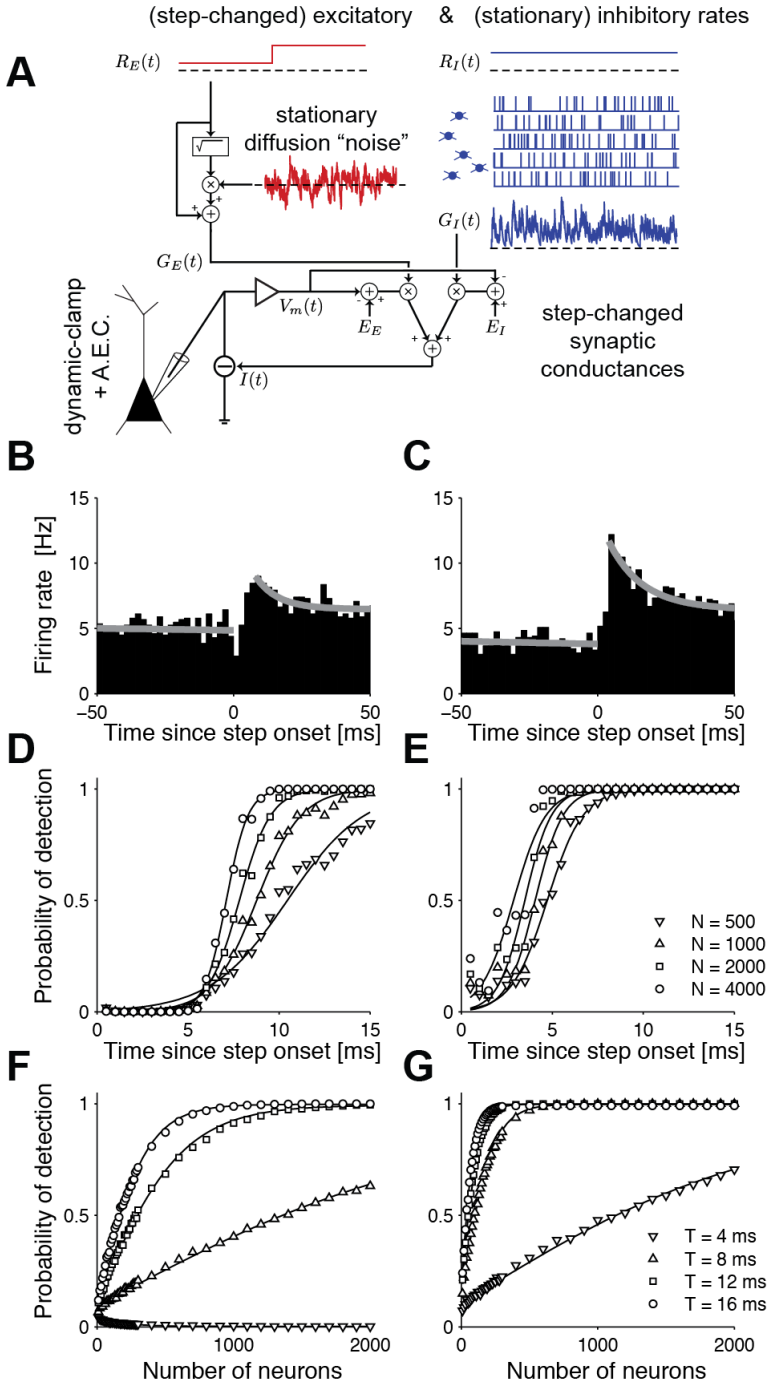

Figure 9: The dynamical response underlies fast tracking of step-changes in presynaptic input rates. We replaced the sinusoidal modulation of the recreated excitatory presynaptic rate with its step-increase (**A**). As apparent from the PSTH (**B**, **C**), the instantaneous output firing rate reacts to a 5% (**B**, **D**, **F**) or 10% (**C**, **E**, **G**) step increase in the presynaptic rate, much faster than inter-spike intervals (*i.e. ~200 ms*). We then set a conventional output detection threshold and mimicked by means of successive PSTH estimates (*i.e.* over 500 to 4000 repetitions) a signal received by a downstream observer (*i.e.* receiving inputs from a population of 500 to 4000 neurons). Doing so, we inferred the probability of postsynaptic detection of the presynaptic step-change and found it increases for wider detection windows (*i.e.* 4-16 ms; **D**, **E**) and larger population size (**F**, **G**). The solid lines are optimal fits with sigmoidal or hyperbolic tangent functions.